Lund University

Faculty of Science

The development of scanning X-ray diffraction phase mapping techniques using automated Rietveld refinements.

Author:
Johannes Brask

Supervisors:
Fredrik Lindberg
Jesper Wallentin

Diploma work

Dep. of synchrotron radiation, Lund University

&

Swerea KIMAB

LUND
UNIVERSITY

Contents

List of Acronyms

bcc body centered cubic

bct body centered tetragonal

fcc face centered cubic

M Martensite

Q&P Quenching and partitioning

R.A Retained austenite

SXRD Scanning X-ray diffraction

XRD X-ray diffraction

Abstract

A methodology for determining inhomogeneities in microstructural features has been established using scanning X-ray diffraction (SXRD) and automated Rietveld refinements. The method has proven successful for spatially resolved quantitative phase analysis or "phase mapping" of retained austenite on a variety of martensitic steel samples, including carbon case-hardened steel bars and quenching and partitioning (Q&P) steel sheets. In addition, the mechanical stability of retained austenite was investigated in bend tested (Q&P) steels after various loading conditions. The results showed a decreasing austenite content from 7.9 wt% to 0 wt% after fracture. The phase distribution was further investigated using SXRD measurements on the cross-sectional area in the region of the bend, indicating an uneven distribution of retained austenite with higher concentrations in the compression side.

1 Introduction

The discovery of X-rays and their interaction with matter has led to enormous insight in the field of crystallography and material science in general. Through the development of X-ray diffraction (XRD), in the early part of the 20th century, pioneers such as Max von Laue and Lawrence Bragg could probe atomic arrangements of crystalline materials. Initially single crystals were solved followed by more complex structures such as the double helix of DNA [1].

The correlated analysis procedure, where the angular distribution and intensity of the scattered X-rays were evaluated, was by no means trivial and required a great deal of effort. In the late 1960s Hugo Rietveld established a methodology in which the crystal structures of powders could be solved or "refined" using the least squares fitting approach [2]. In this way powder or polycrystalline diffraction data with overlapping Bragg peaks could be interpreted in a simple and elegant manner.

Today, the possible usages of XRD are diverse and applies to many fields of science. In regard to metallurgy the method is frequently applied in measurements of grain size, residual strains and furthermore, which is the focus of this work, quantitative phase analysis. In certain metallic components, containing multiple microstructural features, a conventional approach of single XRD measurements is however, no longer adequate in complete material characterizations. To investigate microstructural variations in such materials an extension to the XRD technique is necessary, in which grids of XRD measurements are conducted across two dimensional areas. This method, known as spatially resolved, or scanning XRD (SXRD) has been successfully established to study phase and residual strain distribution in metals and semiconductors [3, 4].

There are however many challenges associated to this method, in particular the subsequent computer analysis process where large XRD data sets must be evaluated. For single XRD measurements quantitative phase analysis can be achieved using standard Rietveld refinements. For SXRD measurements however, with increasing data sets, individual refinements become increasingly difficult and time consuming. In recent years a solution has been developed in which batch data processing is used to automate the Rietveld refinement process which allows for spatially resolved phase mapping [5].

This work aims to establish a simple SXRD phase mapping methodology, using a lab diffractometer, for the possibility of industrial usage. This includes the experimental development of the technique and the creation of an automated refinement strategy to successfully perform microstructural phase mapping. To create a diverse method several martensitic steel sam-

ples with different geometries will be investigated where the soft retained austenite phase is distributed inhomogeneously. Case-hardened steel bars and bend tested quenching and partitioning (Q&P) steel sheet samples will be studied.

The developed SXRD methodology should not be restricted to the measurements of retained austenite in steel components. Therefor a diverse analysis procedure using Rietveld refinements is used in which other microstructural features can be included. It should further be applicable to other metals and solids.

2 Theory

In this section a theoretical background is given to the results presented in this thesis. This includes a basic theory of crystallography and X-ray diffraction with emphasis on the subsequent data analysis process of Rietveld refinements. In addition, the underlying functions of the programs used in this work are explained, where single and multiple Rietveld refinements have been performed on SXRD data.

2.1 Crystallography

2.1.1 Crystal symmetry

The symmetry of the atomic arrangement in crystals were proposed, before the emergence of X-ray diffraction, by studying the symmetry and phases of a large group of monocrystalline solids found in nature. Considering the geometrical restrictions in the possible arrangement of atoms in crystalline solids, there is a limited number of possible configurations in three-dimensional space. These make up a total of 230 space groups. Each space group is, in turn subdivided into 14 Bravais lattices, 32 point groups and finally seven crystal systems or "families" out of which the cubic and hexagonal are the most common in metals [6].

Along with most solids, metals are not monocrystalline but consists of several crystallites or grains. Each individual grain can be thought of as a monocrystalline unit with a given orientation in the structure. The grains may have a random distribution or, because of mechanical stresses induced during manufacturing, a preferred orientation, known as texture.

In X-ray diffraction measurements variations in unit cell dimensions and interplanar spacings d between different (hkl) atomic planes affect the nature of the recorded scattering events. Differences in (hkl) multiplicity (together with the chemical composition of the sample) determines the relative intensity of the Bragg peaks in the obtained diffraction patterns. In addition, the planar separation d will affect their angular distribution. The possible presence of texture in the sample may also have a large effect on the relative intensity of the various Bragg peaks in a diffraction pattern and must therefore be considered when measuring polycrystalline samples [7].

2.1.2 Phase transformations

For a given solid, such as steel, the Bravais lattice symmetry, or "phase", may change as a result of a mechanical or thermal influence, in which there is a shift from the thermodynamical equilibrium of the system. These microstructural changes are of utter importance in material

science since they effect crucial material parameters such as mechanical performance. In metal production, for a given alloying composition, the subsequent rolling and heat treatment processes can be manipulated in order to control the strength and formability of the finished product.

Phase transformations will occur if a system, at a given energy, can "relax" into a state lower energy, and thereby fulfilling the strive to reach a minimum energy state. The shift to a lower energy state is realized by the combined rearrangement of atomic positions across the crystalline structure. The process can be understood in terms of thermodynamics and kinetics which explains the amount of energy that the system is reduced by (known as the driving force of the transformation) and the mechanical process, such as the particle nucleation of the new phase [8].

In Iron there are three different phases (allotropes) in the solid state, namely the α-ferrite phase which has a bcc cubic structure and is stable up to 910 °C, the γ-austenite phase with an fcc structure (910-1395°C) and the bcc δ-ferrite phase, stable between 910°C to the melting point at 1538°C [9]. Iron however, does not have desirable mechanical and structural properties which are realized by introducing interstitials such as carbon, and other alloying elements, to the iron matrix. The resulting materials are classified as steel. Interstitial alloying with carbon is possible since the carbon atom is 1/30 the size of the iron atom and can therefore "fill" the cavities (interstices) between the iron atoms.

There is however a big difference in solubility of carbon for the various phases. Even though the austenite fcc phase has a higher packing density, it contains larger cavities between the iron atoms than the ferrite bcc phase, increasing its solubility of carbon [10]. The austenite phase can contain up to 2% carbon while the bcc ferrite phase contains a maximum of 0.025% [9]. The allotropic transition from the carbon enriched austenite phase upon cooling is the most important part in steel manufacturing. If the cooling rate is slow, the carbon atoms diffuse from the bulk of the steel resulting in the relatively soft α ferrite phase. If the iron cooled rapidly or "quenched" however, the carbon atoms are locked into the crystal structure, forcing an elongation of the bcc phase to a hard body centered tetragonal (bct) structure known as martensite. The resulting materials are referred to as hardened or martensitic steels. The unit cells of the austenite, ferrite and martensite are shown in figure 1.

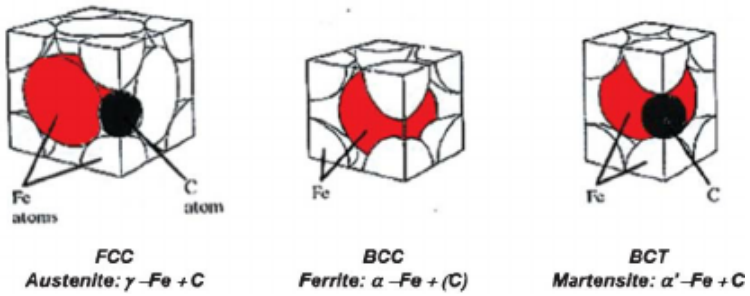

Figure 1: The fcc austenite, bcc ferrite and bct martensite phases of steel showing the positions of the Fe and C atoms in the unit cells. Image taken from [10]

All martensitic steels studied in this work however, have a low carbon content. Therefore, the elongated bct structure is not formed during quenching, which instead results in a cubic bcc martensite.

2.1.3 Retained austenite

Austenite may be retained in hardened steels after the quenching process such that the formed microstructure contains a combination of martensite and austenite. The amount of retained austenite is determined by the chemical composition of the steel, the rate of cooling and the lowest temperature reached in this process [7]. The introduction of alloying elements and carbon will increase the mass or "weight" percent (wt%) retained austenite since it is accompanied by a depression of the temperature at which martensitic transformation starts (the M_s temperature). Additionally, the remaining fraction of retained austenite is dependent on the treatment of the steel after quenching. The heat and cooling process or mechanical deformation may introduce enough energy (the driving force) for transformation to martensite.

Due to its softer properties in relation to the hard martensite phase, a quantification of the austenite concentration and its distribution is crucial to make predictions regarding the mechanical performance of the finished steel product. In the simplest approach optical microscopy is used since the retained austenite grains are distinguishable from the martensite grains for a polished and etched sample. This process however, becomes increasingly difficult for lower austenite contents. A higher precision, quantitative alternative, is realized through the usage of X-ray diffraction [7].

2.2 X-ray diffraction (XRD)

2.2.1 Background

X-rays, which were discovered in 1895 by Willhelm Röntgen, were not however, immediately recognized as electromagnetic radiation. This was established by studying their interaction with matter which led to the development of X-ray spectroscopy. It was through the early work of Max von Laue and Lawrence Bragg that X-rays became the primary tool for investigating the arrangement of atoms in solids. With this new method, a crystallographic "record" could be established, based on the theoretical framework of the 230 geometrical space groups which were earlier theorized by Fedorov, Schoenflies and others [1].

The versatility in usefulness of X-rays stem from their interaction with matter, which, due to their short wavelengths (similar to the interatomic distances) allows for interactions with the atomic structure of solids. As coherent scattering from millions of atoms occur simultaneously, from a small region, the progression of the X-ray waves will be highly dependent on the phenomena of interference. As X-rays of a certain wavelength λ pierce a crystalline solid, they may scatter of the combined stacking of a certain (hkl) plane, depending on the incident angle θ. The scattering events gives rise to constructive and destructive interference depending on the phase difference between the scattered waves. If the phase difference is $n\lambda$, where n is an integer, the waves will interfere constructively, if not, they will cancel each other out through destructive interference. This relation is described by Bragg's equation [6],

$$n\lambda = 2d\sin\theta \tag{1}$$

where $2d\sin\theta$ is the path difference between the scattered waves and n is the order of reflection. In XRD measurements the first order of reflection is generally studied such that $\lambda = 2d\sin\theta$. The relation is illustrated in figure 2.

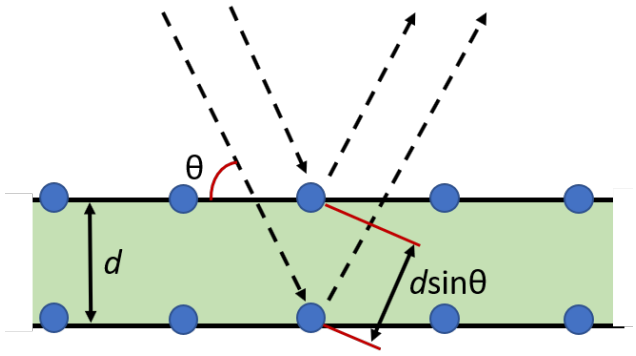

Figure 2: Illustration of the Bragg relation where the incident angle θ is related to the distance d between two atomic planes for X-rays of a fixed wavelength.

The interference phenomena give rise to scattering at discrete angles from the different planes in the lattice. Since the generated X-rays in an XRD experiment are in the shape of a spot, the diffraction will give rise to a pattern of such spots, if recorded by a photographic film, known as the reciprocal lattice [11].

The obtained XRD patterns will appear different depending on the material that is being studied. For monocrystalline solids the positions of the spots in the reciprocal lattice are directly related to the distances between various (hkl) planes and their orientation. In polycrystalline solids (or powders) however, the crystal structure is subdivided into grains/crystallites in which the atomic planes are randomly oriented. This causes a distribution in the scattering from certain (hkl) planes around a given 2θ scattering angle, giving rise to the characteristic Debye-Scherrer rings. Figure 3 illustrates the difference between the obtained XRD patterns from a monocrystalline (left) and polycrystalline/powder sample (middle) together with the resulting 2θ diffractogram (right). In the simplest case in polycrystalline XRD, where a 1D detector is used, a row of the Debye-Scherrer rings is scanned, where the intensity over a 2θ interval is recorded. The diffraction peaks are often referred to as Bragg peaks and result from the scattering of individual families of (hkl) planes.

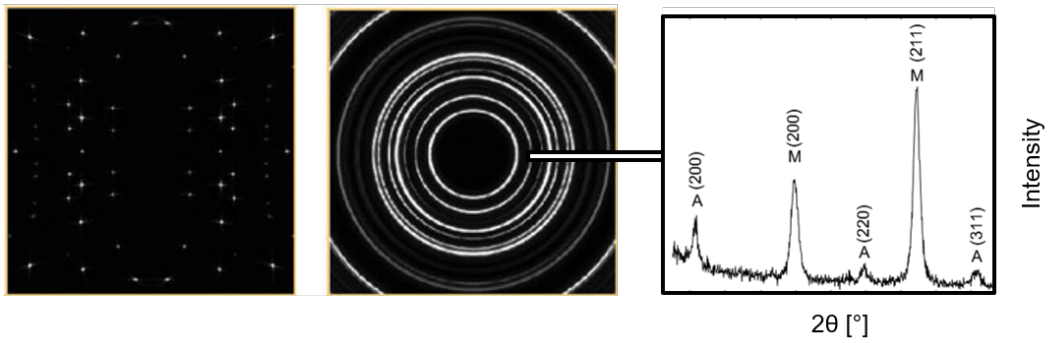

Figure 3: The difference between the monocrystalline (left) and powder/polycrystalline (middle) X-ray diffraction patterns. The resulting 2θ diffractogram is shown to the right. Figure adapted from [12]

2.2.2 X ray diffractometer

XRD measurements can be performed using a lab diffractometer, consisting of an X-Ray tube (where the radiation is generated), a sample stage to hold the samples and a detector to measure the varying intensity of the scattered X-rays. The diffractometer schematics is

shown in figure 4. The figure illustrates a certain measurement geometry used in this work, in which the source and detector moves simultaneously during a 2θ scan, known as the coupled 2θ or θ-2θ method.

By synchronizing the movement of these components, such that the detector only measures the scattering angles which are twice the incident angles, the scattering vector Q, which is perpendicular to the atomic planes, is kept perpendicular to the sample surface. This means that all atomic (hkl) planes which contribute to the recorded diffraction pattern are parallel to the surface of the sample. It is also important to keep in mind that the penetration depth of the X-rays varies with different materials for a given energy. For metals this can be a limiting factor where the X-rays only measure a thin surface layer, which may vary structurally from the bulk. In this work steel samples have been measured using a Cu Kα; 40 kV radiation source resulting in a penetration depth of a few μm. The size of the XRD spot and thus the resolution of a SXRD measurement, can be controlled by changing the nozzle of the X-ray tube.

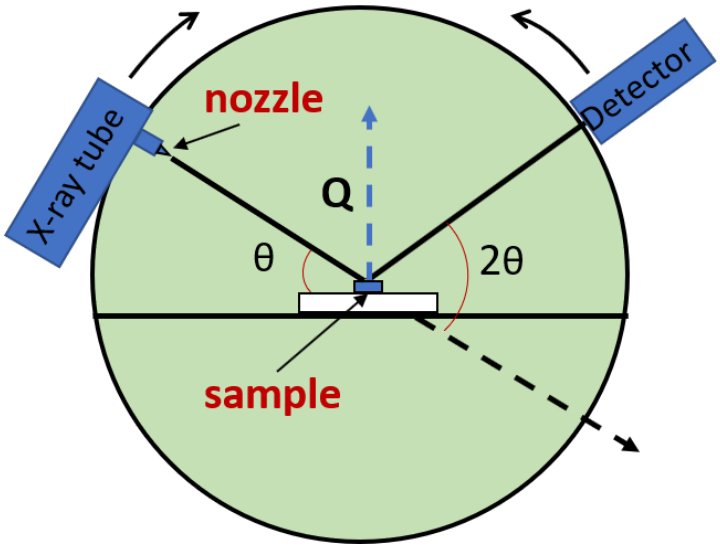

Figure 4: X-ray diffractometer schematics showing the coupled 2θ geometry

2.2.3 Scanning X-ray diffraction (SXRD)

In SXRD, sequential XRD measurements are conducted on a line or a two-dimensional area on a sample in order to map the spatial distribution of certain crystalline features. This includes the possibility to map phase distribution [3] and possible crystal structure defects such as residual strains [4]. Figure 5 shows the schematic of a simple SXRD area scan where a 10×10 grid has been generated in which each point contains a diffractogram. The possible resolution of the mapping is limited by the X-ray source. The lab diffractometer used in this

work can achieve resolutions up to 0.3 mm and is therefore suited to measure variations in microstructure on a macroscopic scale.

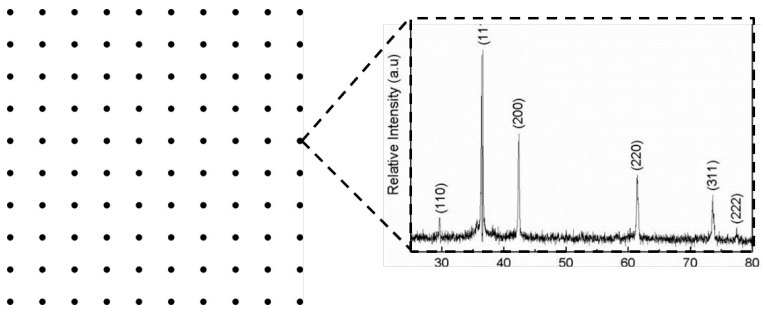

Figure 5: The outline of a SXRD measurement where each point in the scanned grid contains a diffractogram.

In SXRD measurements the number of collected diffractograms quickly exceed the practical limit for "manual" analysis of subsequent diffraction patterns. A batch data processing approach is therefore necessary to automate the procedure. In the upcoming section the quantitative XRD data analysis process of Rietveld refinements is explained together with the pieces of software used in this work. This includes the General Structure Analysis System (GSAS) [13] and Multiref [5], which automates the Rietveld refinement process.

2.3 Quantitative XRD data analysis

2.3.1 Rietveld refinement

The Rietveld refinement method was established by Hugo Rietveld in 1967 to identify overlapping Bragg peaks in neutron powder diffraction experiments [2]. The method provides an elegant solution to solve or "refine" the crystal structure of a material from the position, shape and relative intensity of the Bragg peaks in a diffraction pattern. The method is composed of two parts. First a model diffraction pattern is generated, based on known instrument and sample parameters, to match the experimental data. Then the model is corrected, using the least squares method, such that the difference is minimized. By subsequently "tuning" different parameters, information about the crystal structure, such as unit cell parameters, crystallite/grain size, strain, preferred orientation and phase fractions, can be extracted from the model. The refinement process can be subdivided into three categories where the position, relative intensity and shape (profile) of the Bragg peaks are corrected.

- Peak position

  The angular 2θ position of a Bragg peak is directly related to the distance d between the atomic planes from which the scattering occurs, and the wavelength of the radiation,

according to Bragg's law (see equation 1). Therefore, it is necessary to know the composition and crystallographic identity of the studied sample, to start the refinement process. The theoretical model will positions the Bragg peaks according to space group, lattice parameters and atomic positions, at certain 2θ values. Initially, however, there are often displacements between the model and the experimental data. Figure 6 shows the initial stages of the Rietveld fitting process for a steel sample, with four Bragg peaks from the martensite (M) and austenite (A) phases. Initially the theoretical (dots) and experimental (line) Bragg peaks are not located at the same 2θ values, which is clearly visible for the A (220) peak (as can be seen in the insets of figure 6a). This is caused by a possible deviation between the theoretical and actual unit cell dimensions or a sample height misalignment, producing faulty 2θ values. During Rietveld refinement the misalignment and unit cell parameters are corrected in the least squares fitting process causing the positions of the theoretical Bragg peaks to better match the experimental data (see figure 6b). There may also be defects in the crystal structure, such as strain, which alters the interplanar spacing between the atomic (hkl) planes and in turn causes shifts in the diffraction patterns [14].

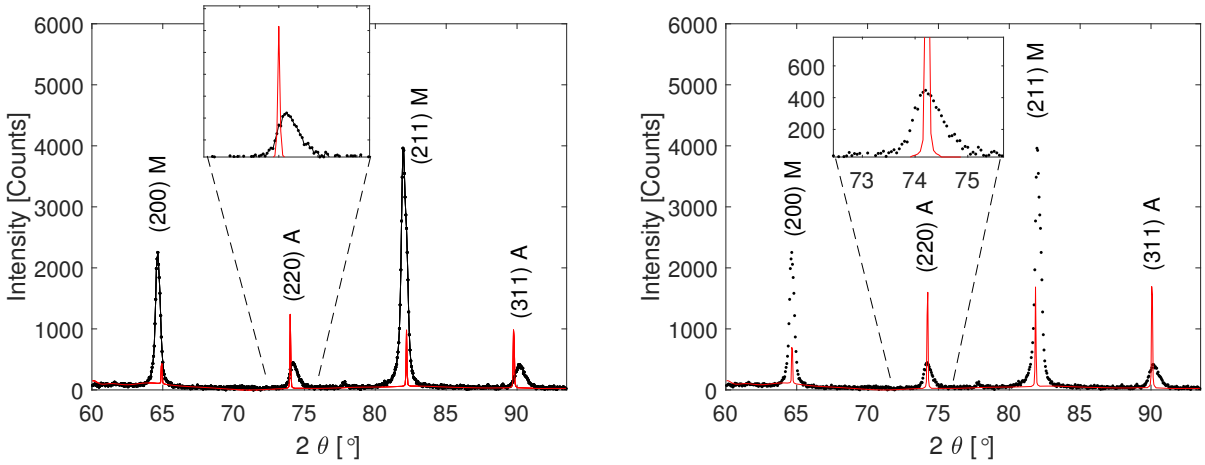

Figure 6: The initial correction in the Rietveld refinement process of a diffractogram obtained from martensitic steel a) The position of the Bragg peaks for the theoretical model (line) poorly match the experimental data (dots) which is highlighted for the austenite A (220) peak. b) After refining sample misalignment and unit cell dimensions, the peak positions match.

- Peak intensity

  The absolute intensity of the Bragg peaks of the experimentally obtained X-ray diffrac-

tion pattern is dependent on the sample geometry, the intensity of the source and the quality of the detector. The relative intensities, however, are instrument and source independent and reflect the differences in scattering events for various (hkl) planes in the crystal structure of the sample. The plot displayed in figure 6b shows that there is a clear difference in relative intensities between the model and the experimental data. The relative intensities of the theoretical Bragg peaks are based on the chemical composition of the sample and the multiplicity of the various (hkl) planes. If there are more than one phase present in the sample microstructure (such as in steel) and their mass fractions differ, then the relative intensity between Bragg peaks of the same multiplicity and atomic composition will vary. To fit the model accurately it must be scaled to take into account all above mentioned factors (see figure 7a). Scaling the height of the theoretical Bragg peaks is however not sufficient in making any qualitative predictions regarding phase fractions, due to sample and instrument peak broadening effects.

- Peak shape (profile)

  The shape or profile of a Bragg peak may vary with different radiation, XRD geometry and sample properties. In principle, according to Bragg's law (equation 1) the scattering angle θ is only dependent of the interplanar distance d when using monochromatic radiation. In a perfect crystal, where d is invariable, the constructive interference should be limited to a precise θ value, resulting in a Bragg peak described by the Dirac delta function. In a real crystal however, there are lattice imperfection causing small changes in d as well as a finite number of atomic planes. In polycrystalline samples, a reduction in grain size causes an increase in the resulting peak width. Fewer atomic planes results in a limitation in the destructive interference of angles which are close to the Bragg angle. Similarly, the presence of micro strains stretches the interatomic bonds creating small positionally dependent changes in d which widens the Bragg peak. As a result, the maximum intensity of the obtained Bragg peaks may vary due to the above-mentioned factors, but the area under each peak is however constant.

  The X-ray profile is generally complex and may depend on several parameters including the source, the receiving slit and the specimen, which results in an asymmetric Gaussian function [15]. In addition, the Lorentzian emission profile of the Cu K alpha radiation (used in this work) contribute to a broadening of the profile at low intensities. Bragg peaks are profiled by a convolution between a Gaussian and Lorentzian function (namely the Voigt function). The convolution however, is too numerically intensive to be practical in a Rietveld refinement process. Therefore the "pseudo" Voigt is often used, which is the weighted sum of the Gaussian and Lorentzian functions [15] (see figure 7b).

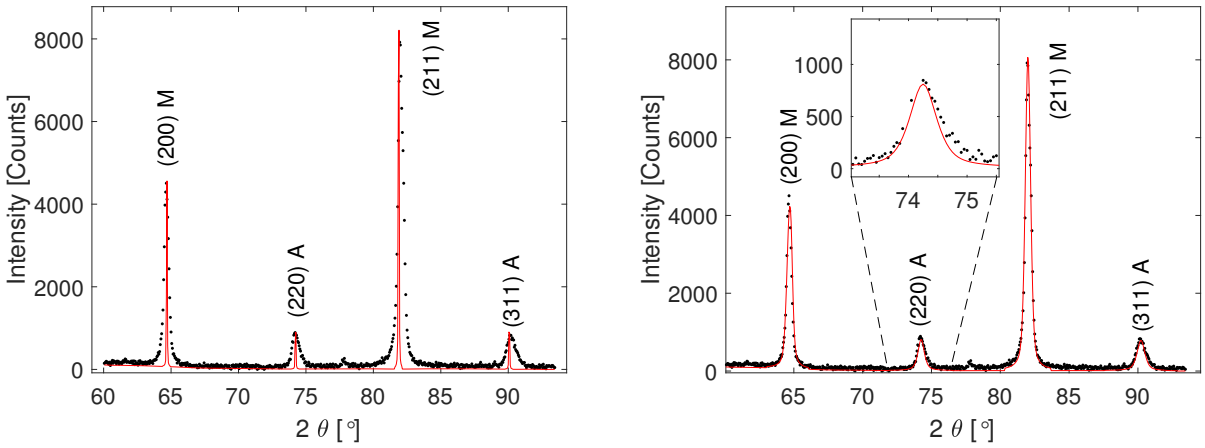

Figure 7: The final corrections to relative peak intensity (a) and peak profile (b) in the Rietveld refinement process.

After the profile has been refined to match the experimental data, the volume fractions and corresponding weight fractions of various phases can be determined. The amount of a certain phase in a sample is directly proportional to the number of scattering events from that phase during the XRD measurements.

This could be understood using the diffraction patterns of martensitic steels displayed in figures 6 and 7, where the austenite and martensite phases are present, as an example. If there is no preferred orientation or any other phases in the steel, the volume fraction V_A of retained austenite is given by the following equation [7],

$$V_A = \frac{I_A^{hkl}/R_A^{hkl}}{I_A^{hkl}/R_A^{hkl} + I_M^{hkl}/R_M^{hkl}} \tag{2}$$

where I^{hkl} and R^{hkl} are the relative integrated and theoretical intensities of Bragg peaks corresponding to certain (hkl) planes.

The weight fraction w of each crystalline phase is often calculated due to the difference in atomic densities d of the various crystalline phases. The weight fraction for phase k in a mixture of phases $k\prime$ is given by the general equation [16]

$$w_k = \frac{v_k d_k}{\sum_{k\prime=1}^{K} v_{k\prime} d_{k\prime}} \tag{3}$$

where the density d_k is given by $Z_k M_k / U_k$ where Z_k is the number of atoms per unit cell, M_k is the mass of each atom and U_k is the unit cell volume. The weight fraction is often

represented with a denominator of 100, in percentage by mass or weight percent, denoted wt%.

2.3.2 GSAS EXPGUI; Rietveld refinement software

The general structure analysis system (GSAS), performs Rietveld refinements on neutron or X-ray diffraction data for mono/polycrystalline and powder samples [13]. The refinements are controlled via the user interface EXPGUI. In order to understand the results presented in this project, it is important to detail certain aspects of the software and the sample parameters which are refined when analyzing XRD data. Initially an "experiment" EXP file is created which includes unit cell parameters a, b, c, angles α, β and γ, space groups and atomic positions of each phase present in the sample. These are simply uploaded from a crystallographic database [17]. The EXP file also contains information about which parameters to refine (which is controlled via the EXPGUI interface) and is therefore continuously rewritten during the refinement process. In addition, an instrument (INS) file is uploaded, containing information about instrument parameters such as the wavelength of the radiation. The combining EXP and INS files generates the initial theoretical model which is discussed in section 2.3.1. In order to obtain relevant crystallographic information, the sample parameters are sequentially refined, using the least squares fitting process, such that the Bragg peaks positions and profiles better match the experimental data. The evolution of the theoretical model can be viewed, together with the experimental data, in a 2θ/intensity plot. The meaning and underlying function of the most important parameters refined in this project are listed below.

- Background

  The Background of the experimental signal is important to include in the fitting process, especially when comparing the integrated intensities of the Bragg peaks. GSAS offers several background functions. In this work the most common approach, the Chebyshev polynomial function [13] is used in all refinements.

- Zero shift

  The zero-shift parameter allows for refinement of possible misalignments in the sample height, which shifts the 2θ angles of the resulting Bragg peaks.

- Scale factors

  In order to correct the intensity of the Bragg peaks in the model to the experimental diffraction pattern, the scale factors are refined. This is done to account for instrument parameters and the possible difference in wt% (equation 3) between different phases in the samples. GSAS offers the possibility to scale each phase separately which is the

basis for quantitative phase analysis. The scale factor for each phase S_{ph} incorporates the volume of the unit cell and the theoretical relative intensity of the different Bragg planes together with a correction for the varying total intensity of the scattering. The weight fraction W_p is then calculated by comparing S_{ph} of one phase to the sum of scale factors from all phases, using the following equation

$$W_p = \frac{S_{ph} m_p}{\sum_{p=1}^{N_p} S_{ph} m_p} \tag{4}$$

where m_p is the mass of the Unit cell. W_p is then converted to wt% by a factor of 100.

- profile parameters

  The profile parameters decide the appearance the resulting weighted pseudo Voigt function which should match the shape of the obtained Bragg peaks. The full width at half maximum (FWHM) is dependent on the angle of reflection (θ), which is considered by introducing the Gaussian Caglioti function:

$$\text{FWHM}^2 = U\tan^2(\theta) + V\tan(\theta) + W \tag{5}$$

  where U, V and W are constants. In addition, two parameters; LX and LY are refined to account for the Lorentzian peak broadening from finite grain sizes and microstrains in the crystal structure.

- Texture

  The presence of texture in a sample can be included in the refinement process in different ways. GSAS offers the possibility to include preferred orientations from various (hkl) planes in the same phase, using the March Dollase approach [18].

2.3.3 Multiref; automated Rietveld refinement

Position resolved or in situ XRD experiments results in large data sets where separate Rietveld refinements, using a program like GSAS, is too time consuming. The Multiref software offers the possibility for automated Rietveld refinements of multiple powder or polycrystalline diffractograms [5]. Multiref is written in the numerical computing programming language MATLAB [19] and used GSAS as the Rietveld refinement engine.

A refinement strategy can be created for many diffractograms, where different sample and instrument parameters are refined. In this way it is possible to perform Rietveld analysis on SXRD data. The software architecture is displayed in figure 8. Initially one or more

representative diffractograms from the SXRD measurement is refined in GSAS which results in an EXP file which is used as a reference (or staring point) for the additional XRD data. The EXP file is imported to Multiref together with the INS file and the diffraction data. When the Multiref script is run, the diffraction data is send to GSAS which refines each diffraction pattern based on the reference EXP file. In addition, the EXP file can be rewritten to add more parameters for refinement. The refinement can be conducted in steps or "cycles" in which more parameters are added. By doing so the refinement process can be more easily controlled and conditions can be introduced between each cycle such that certain diffractograms, which produce divergence in the least squares fitting process, can be excluded from the restoring refinement cycles. An example could be to refine the background and unit cell parameters in the first cycle, then adding scale factors, profile parameters and texture in following cycles. After the refinement process the obtained sample parameters are saved using the Multisave script and then plotted in two-dimensional color plots using Multiplot. The results from the refinements, such as scale factors and wt% values can in this way be represented figuratively.

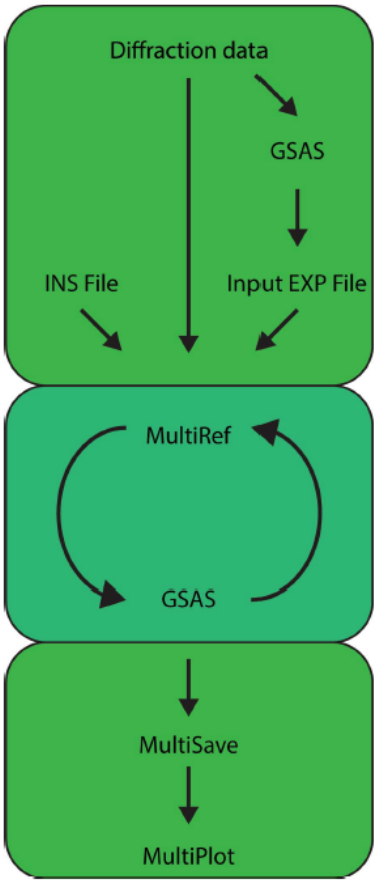

Figure 8: The architecture of the automated Rietveld refinement software Multiref. Image taken from [5]

3 Method and materials

In this section a short background is given regarding the martensitic steels and samples studied in this work, followed by the experimental procedure of the position resolved "scanning" XRD measurements. In addition, the subsequent computer analysis procedure is outlined, where single Rietveld refinements were performed using the GSAS EXPGUI software [13] and the succeeding automated Rietveld refinement software Multiref [5].

3.1 Materials

3.1.1 Case hardened steel

In order to achieve good strength and toughness properties in steel machine parts (such as gears) the surface, or "case", is often hardened via carbon case hardening, in which carbon atoms are added to the surface layer in a diffusion process. As opposed to through hardening, the case-hardened components achieve high compressive residual stresses, which increase impact-fatigue resistance and thus the lifetime of the steel component [20]. In addition to the hard metastable martensite phase carburization also produces undesired microstructural changes, such as carbides, internal oxidation and (which is the focus of this project) retained austenite.

3.1.2 Quenched and partitioned (Q&P) steel

The desired combined properties of high strength and ductility in steels can be realized by combining the hard and brittle martensite phase with the soft and ductile austenite phase in the steel microstructure. This requires a stabilization of the metastable retained austenite phase at room temperature which is achieved in martensitic steels using the quenching and partitioning heat treatment process [21]. The steel is austenized and quenched to a temperature below the martensite start temperature M_s and above the martensite finish temperature M_f, where some retained austenite has not yet transformed to martensite. The steel is then additionally tempered above M_s to partition carbon from the supersaturated martensite to the retained austenite which is then stabilized at room temperature. In sheet steels the carbon enriched retained austenite phase can increase the formability through the transition induced plasticity (TRIP) phenomena in which austenite transforms to martensite during plastic deformation, hindering the movement of slip and dislocations [21].

3.2 Sample preparation

The steel samples studied in this work had undergone various degrees of surface grinding and polishing prior to testing. This procedure could induce austenite to martensite transforma-

tion depending on the mechanical stability of the retained austenite in the samples [22]. It was therefore necessary to chemically remove, a few micrometers of the surface layer of the samples. This was achieved using a piranha etching solution [23], consisting of a 3:1 mixture of sulfuric acid and hydrogen peroxide.

3.3 XRD measurements

The combined scanning and single XRD measurements conducted in this work aimed to investigating the spatial distribution and mechanical stability of retained austenite in steel. The general purpose however, was to establish a methodology for phase mapping using SXRD. Therefore, several measurements were performed on various steel samples with different alloying elements and carbon contents.

Although the influence of other elements in the lattice structure of the steel can influence the number of scattering events in XRD measurements, and thereby the intensity of the obtained Bragg peaks, all steel samples have been assumed to contain only Fe and C atoms. In addition, when evaluating the percent retained austenite by weight, it is assumed that the carburized and Q&P martensitic steels only consist of martensite and retained austenite. The presence of possible carbides is not included in the phase analysis process.

All XRD and SXRD measurements were performed using a Bruker D8 Advance diffractometer [24], with a Cu anode material, generating the Cu Kα_1 (1.54060 Å) and Kα_2 (1.54443 Å) X-ray radiation resulting in a penetration depth of a few μm in steel samples. A coupled two theta approach was employed in each measurement and the resolution (the XRD spot size) was controlled by changing the nozzle of the diffractometer source, generating spot sizes of 1 and 0.3 mm. To obtain mass fractions during phase mapping, a 2θ interval was chosen to contain five Bragg peaks from the retained austenite and martensite phases (see figure 9). These peaks are pronounced and easily distinguishable. In addition, it is favorable to include several peaks in quantitative phase analysis when the microstructure of the sample has preferred orientation [25]. Using Cu radiation this interval is located between 2θ values of 47.5° and 93°. For each scan a step size of 0.05 ° was used with a recording time of 0.5 sec/step when using 1 mm resolution and 1 sec/step when using 0.3 mm resolution. Using continuous scanning the resulting time for SXRD measurements was roughly 24 h for 100 diffractograms.

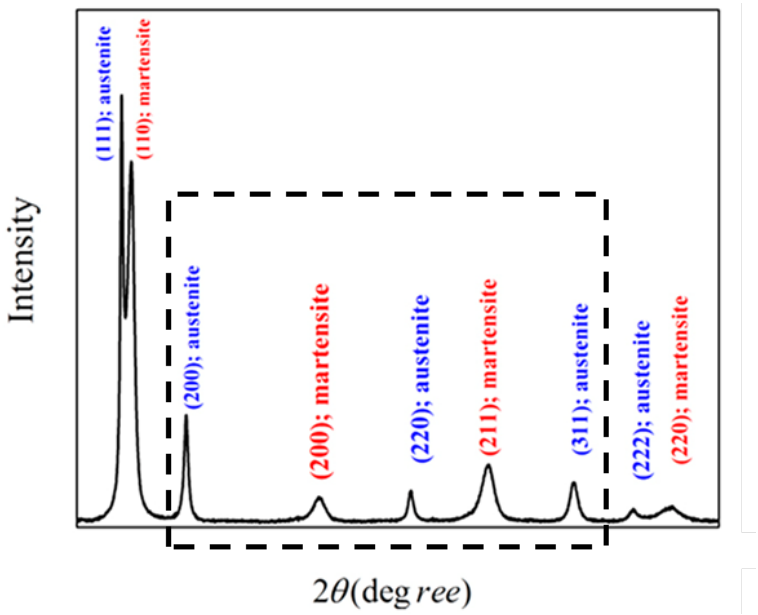

Figure 9: An X-ray diffraction pattern of high carbon martensitic steel containing several austenite and martensite Bragg peaks. The figures illustrate the interval between 47.5° and 93° that was chosen for the phase mapping conducted in this work. Image adapted from [22]

3.3.1 Computer analysis

To perform Rietveld refinements on all obtained XRD patterns from the SXRD phase mapping, a theoretical model was created from known sample and instrument parameters to match the experimental data. This included the wavelength of the Cu Kα_1 (1.54060 Å) and Kα_2 (1.54443 Å) radiation and the lattice constants for the cubic Fe fcc austenite and bcc martensite phases (2.87 Å and 3.44 Å respectively). Together with the atomic positions the unit cell parameters were imported from a crystallographic database [17].

3.3.2 Steel bar 1

To establish the SXRD methodology for quantitative phase analysis of retained austenite a line scan of 100 XRD points was initially conducted over the cross section of a carburized steel bar with a diameter of 30 mm (see figure 10). A 0.3 mm XRD spot size was used.

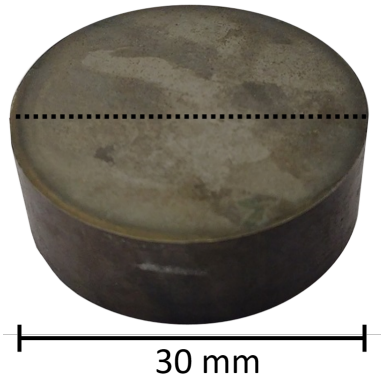

Figure 10: The polished and etched cross section of a carburized steel bar with a diameter of 30 mm. An XRD line scan, resulting in 100 diffractograms, was conducted across the sample, the location is indicated by the dotted line.

A reference pattern, where both austenite and martensite peaks were distinguishable, was chosen from the 100 diffractograms and further refined using the GSAS EXPGUI software. The zero shift, individual phase scale factors and pseudo Voigt profile parameters were all included in the refinement process. No significant texture was found in the sample. All diffraction data was then process in Multiref, using the reference pattern as a starting point. To simplify the refinement process, the obtained zero shift and profile parameters from the reference pattern were used in all the following refinements. Only the unit cell parameters and scale factors were refined for each diffractogram. The resulting scale factor parameters from all 100 diffractograms were then converted to wt% using equation 4.

3.3.3 Steel bar 2

The distribution of retained austenite was also measured on the cross section of an additional case-hardened steel bar (see figure 11) by creating two dimensional SXRD phase maps. The sample had been polished prior to measurements. Initially a 10×10 mm area was scanned using an XRD spot size of 1 mm (resulting in a 10×10-point grid). The region was then concentrated to the edge of the sample were an additional phase map was scanned over a 3×12 mm area using a reduced XRD spot size of 0.3 mm thus increasing the resolution and the grid dimensions to 10×40 points (see figure 11b). To investigate the influence of retained austenite using various sample preparation processes, the initial map of 10×10 mm was repeated over the same region of the sample after chemical etching.

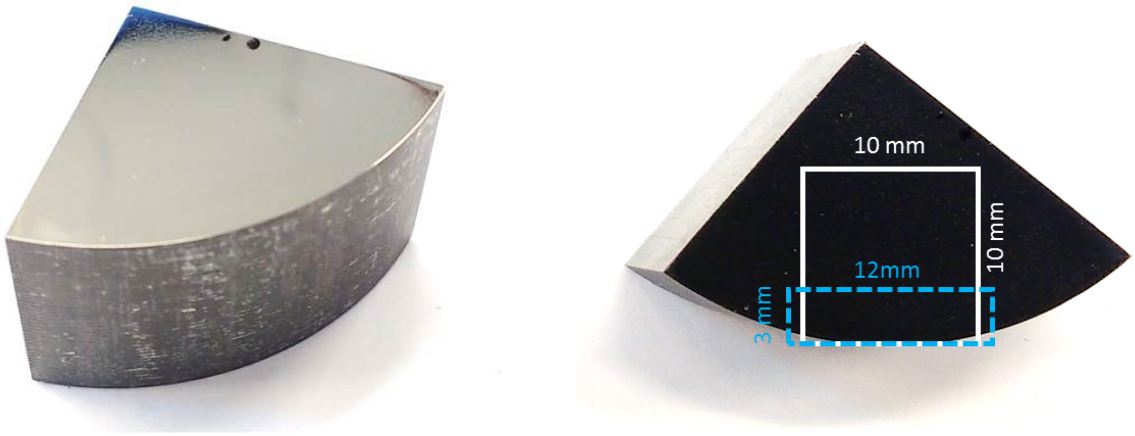

(a) (b)

Figure 11: a) A portion of a case-hardened steel bar with a polished cross section. b) The regions of 10×10 mm and 3×12 mm where SXRD phase mapping was conducted to measure the % retained austenite by weight.

The same procedure of creating a theoretical reference model, as described for steel bar 1, was also employed for all area scans conducted on the second steel bar. The presence of preferred orientation or "texture" was however discovered in the sample. This was therefore included in the refinement process of the reference diffractogram using the March-Dollase approach [18]. Like the strategy used for steel bar 1, the zero shift, profile and additionally the texture parameters, were locked during the automated refinement process such that only the unit cells and scale factors were incorporated in the least squares fitting method.

3.4 The mechanical stability of retained austenite in Q&P sheet steels

The gradual transformation of retained austenite to martensite was investigated in four bend tested Q&P sheet steels using XRD measurements. The samples were 2 mm thick and 5 mm wide, cut from the same steel sheet which had been prepared with flat sheet grinding. Bend testing was performed under four different loading conditions using two loading pins with radii of 15 mm and 0.6 mm to induce a variation in the tensile and compressive strains in the samples. Fracture was initiated on the top of the bend using the 0.6 mm loading pin indicating maximum tensile strain. The bend tested samples are shown in figure 12 where they have been numbered after increasing load. After bending the samples were etched using the piranha solution.

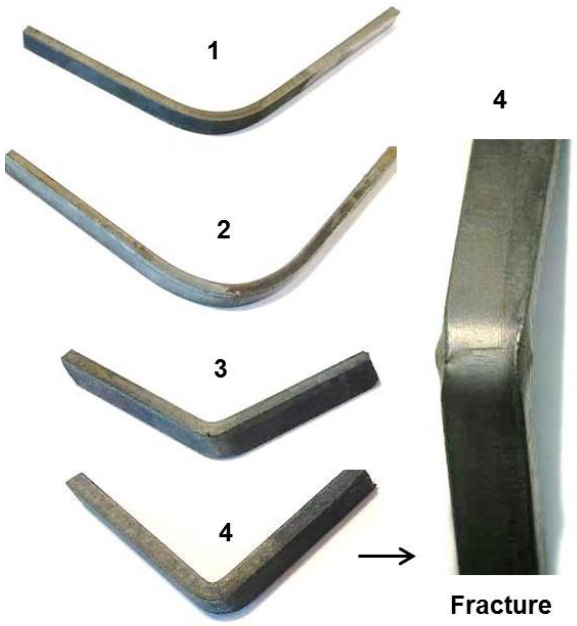

Figure 12: Bend tested Q&P sheet steel samples using a loading pin radius of 15 mm (1 and 2) and 0.6 mm (3 and 4). Fracture was initiated on top of the bend for the forth sample exposed to the highest loading condition.

3.4.1 Single XRD measurements (tension/compression side)

Qualitative XRD phase analysis was conducted on the top of and under the bend (the tension and compression side) of the samples using Rietveld refinement. The compression side however, was only measured for the samples which were bend with the 15 mm loading pin. Using the smaller pin induced a large cut in the impact region of the compression side which may have induced martensite transformation. The 2θ region of the XRD measurements was narrowed down to 47.5°-68.5° to include the most prominent austenite (200) peak and the martensite (200) peak for phase volume fraction comparison (see figure 13).

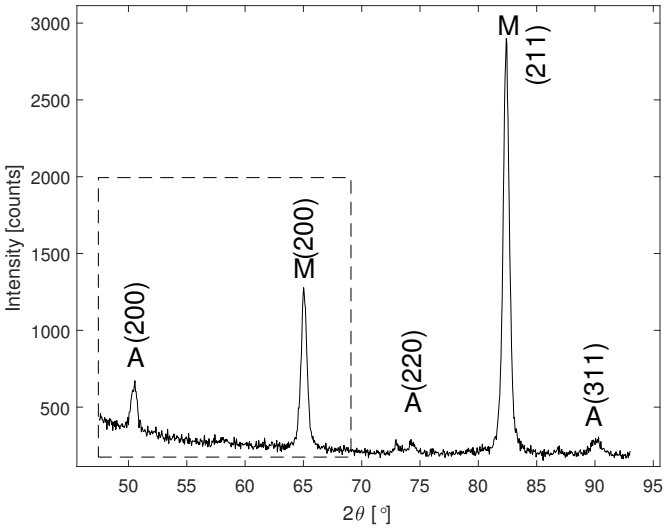

Figure 13: XRD measurements on a Q&P sheet steel sample between 2θ values of 47.5° and 93°. The region was narrowed down to include the retained austenite (200) and martensite (200) peaks during different loading conditions.

3.4.2 SXRD phase mapping (Cross section)

To investigate the spatial distribution of retained austenite through the sheet samples a SXRD measurement was conducted on the cross section of sample 2 which had been bend using the 15 mm bending pin radius. The scanned area was 2.7×4.2 mm, corresponding to 9×14 points (see figure 14) using a 0.3 mm XRD spot size. The cross-section area was prepared using surface grinding, up to 3000 grit sandpaper, and etching, using the piranha solution. Roughly 1 mm was removed from the cutting edge of the sample to reduce the effect of mechanically induced martensite transformation. Scattering was recorded between 2θ values of 47.5° and 93°.

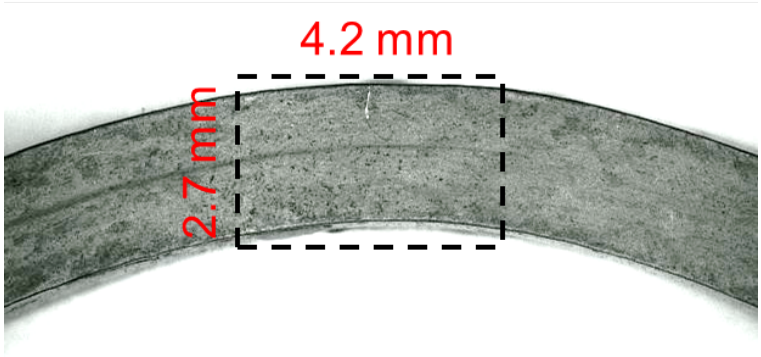

Figure 14: The cross section of bend tested Q&P sheet steel (sample 2) where a 2.7×4.2 mm is indicated for SXRD phase mapping. The surface was prepared using grinding and etching.

4 Results and discussion

In this section, the results obtained from the single and scanning X-ray diffraction measurements are presented. To establish the SXRD methodology, the cross section of two case hardened steel bars were measured, in which the microstructure varies significantly between the carburized case-hardened regions and the bulk. In addition the method was applied to the measurements of the mechanical stability of retained austenite in bend tested (Q&P) steel sheets. This included single "point" XRD measurements on top of and under the bend after various loading conditions and SXRD phase mapping of the cross-sectional region of the bend.

4.1 Spatial distribution of retained austenite in case hardened steel bars

4.1.1 Steel bar 1

A line scan of 100 XRD points, between 2θ values of 47.5° and 93°, was conducted over the 30 mm cross section of a case-hardened steel bar to measure the distribution of retained austenite across the width of the sample. Figure 15 illustrates the line over which the scan was conducted. Two positions are indicated, in the middle (corresponding to the bulk of the bar) and close to the edge of the sample, in the carburized region. The corresponding diffraction patterns are shown to the right. At the bulk the M (200) and (211) martensite peaks are clearly visible together with the retained austenite A (200) and, the less visible, (220) and (311) peaks. At the carburized region, the A peaks are no longer distinguishable from the noise signal, indicating a total absence of retained austenite.

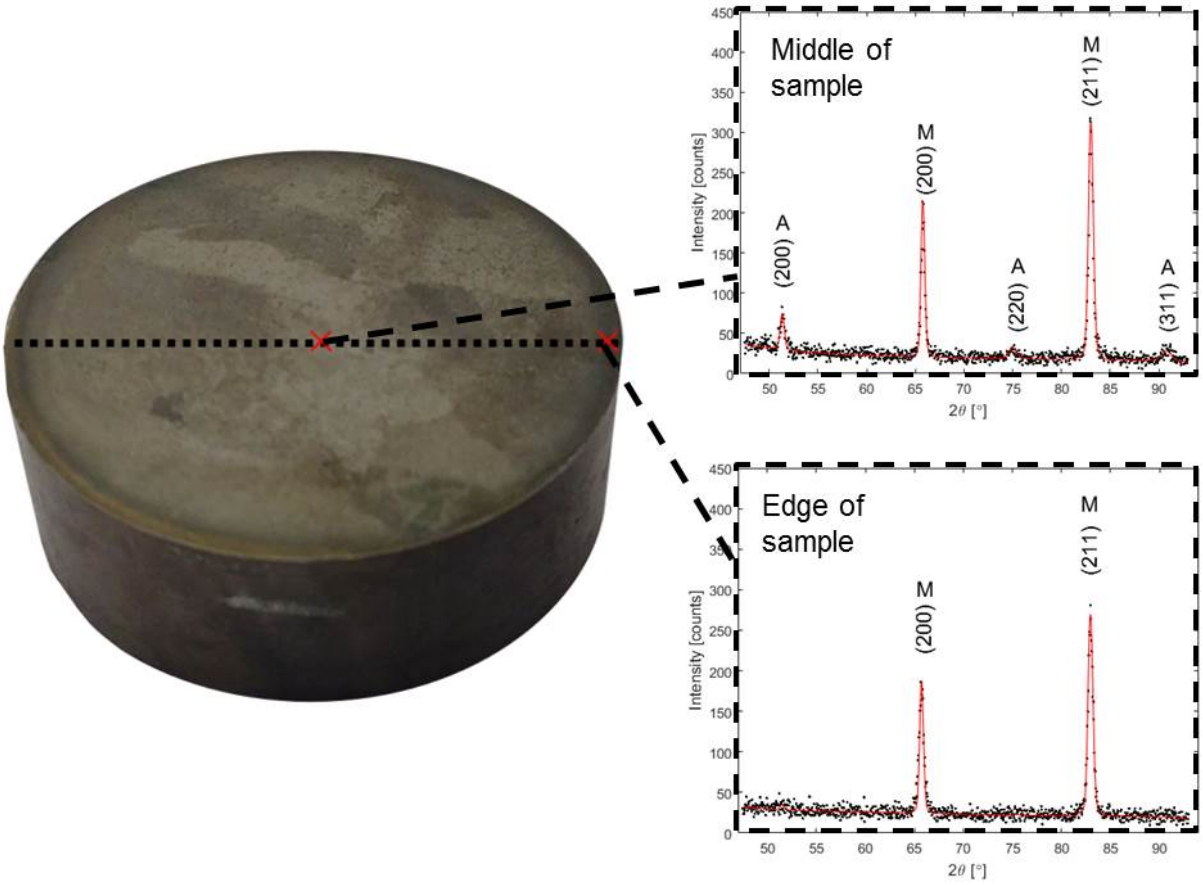

Figure 15: The polished and chemically etched cross section of a case-hardened steel bar where a line scan of XRD points has been conducted across the sample. Two representative diffractograms, from the middle "bulk" and the edge of the sample are shown to the right indicating a total reduction of retained austenite near the sample edges.

The percentage retained austenite by weight (wt%) from all scanned XRD points are shown in figure 16. The graph indicates an uneven phase distribution across the sample diameter, where the retained austenite content starts diminishing close to the edges. Starting from $\sim$ 8 mm towards the bulk, the retained austenite content drops, on both sides from bulk values between 6-14 % to 0 %. For case hardened steels the opposite is expected since the increase in carbon should depress the M_S temperature and thus promote the austenite fraction [20] (as discussed in section 3.1.1). The case-hardened region, located at the last mm of the steel bar edge, should show a dramatic increase in retained austenite. The results from the line scan indicates a possible decarburization process during manufacturing, where carbon has diffused from the outer layer of the steel bar resulting in the reduction of retained austenite.

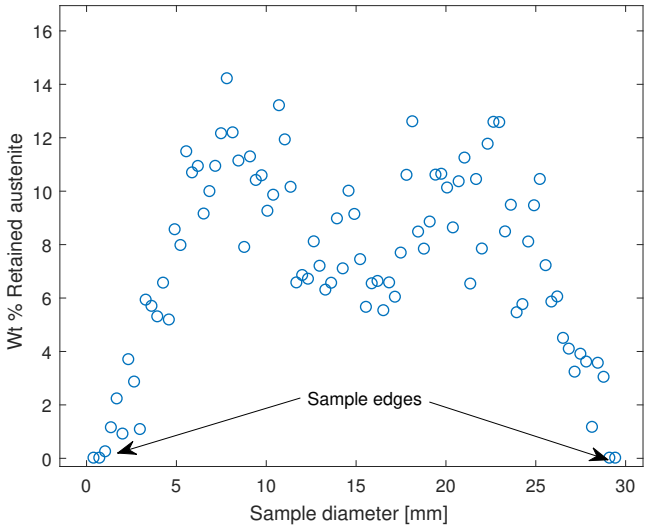

Figure 16: The obtained wt% retained austenite from a SXRD line scan conducted on a case-hardened steel bar, showing a reduction of austenite close to the sample edges.

Since the wt% values for the retained austenite phase are obtained by comparing the integrated peak areas for the austenite and martensite phases (as shown in equation 3) the uncertainty of each value is strongly dependent on the success of the Rietveld refinement process. In using the profile parameters which were obtained from the reference pattern on all diffractograms, any changes in peak profile across the sample will cause a worse fit during the least squares process. Possible inhomogeneities in strain, grain size or texture could therefore not be accounted for in the refinements.

Figure 17 shows the reference pattern (a), which was refined manually, and a diffractogram closer to the edge (b), which was fitted in the automated refinement process. The automated approach has reduced the quality of the fit slightly, which is seen by comparing the insets of the enhanced M (200) peak in each figure. The fit from the automated refinement fail to incorporate some data at low intensity values, the Lorentzian contributions, which may have been caused by smaller grain sizes or micro strains in the lattice at this location of the sample. In addition, there seem to be a small changes in texture or possibly chemical composition, causing a shift in relative peak intensity for the martensite peaks. This can be seen in the M (211) peak in figure 17b which is not fully incorporated by the refined model.

Frølich and Birkedal, established a methodology for the refinement of larger SXRD scans from synchrotron radiation measurements, in which the profile and texture parameters were refined in subsequent cycles after the background and scale factors for polymorphic solids [5]. This approach allows for corrections of the variations in microstructure as discussed

above and is encoded in the Multiref framework. In this project however, a simplification of the refinement procedure has been used to establish a methodology for investigations of macroscopic inhomogeneities in a variety of steel samples.

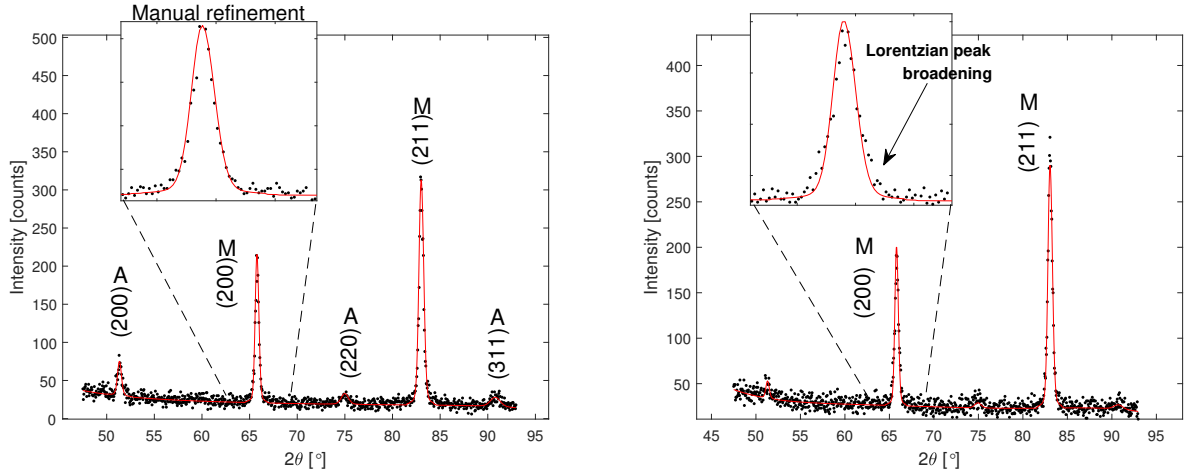

(a) (b)

Figure 17: The XRD data (dots) and resulting fits (line) from the Rietveld refinement process. a) The reference pattern which was refined manually. b) A diffractogram obtained from a position closer to the edge of the sample which was fitted in the automated refinement process. The insets show a slight reduction in the quality of the fit which fails to incorporate Lorentzian peak brocading at low intensity values.

4.1.2 Steel bar 2

Two dimensional SXRD phase mapping was conducted on the cross section of an additional case-hardened steel bar in order to investigate the spatial distribution of retained austenite in the vicinity of the carburized region (close to the sample edge). The wt% retained austenite (R.A) obtained from the 10×10 grid scans before and after etching are displayed as color plots in figure 18. The size of the XRD spot is shown in the upper right corners and the sample edge locations are indicated with dashed lines. The pixels are white at any point where the signal to noise ratio of the corresponding diffractogram was too low or where scattering was recorded from other sources than the sample.

both phase maps any visible deviation in wt% values occurs in the two columns closest to the sample edge, corresponding to the case-hardened area. The remaining "bulk" values are very similar for the sample prior to and after etching with values of 6.0±0.8 wt% and 6.3±0.9 wt% respectively. After etching the sample was positioned in a way which eliminated undesired scattering from sources other than the sample when the edge of the map was scanned. Thus,

the retained austenite in the case hardened region could be measured successfully with values up to 38 %.

The respective wt% values of the two columns closest to the edge vary significantly and the highest values are located on the top and bottom of the columns. This is caused by the difference in geometry for the rounded sample and the square phase map. When a part of the XRD spot misses the sample, the scattering will occur from a smaller region closer to the edge. The fact that the maximum values were obtained from regions where the XRD spot only partly interacted with the sample cross section indicates that there is a gradient in the distribution of retained austenite in the case-hardened region with increasing values towards the edge.

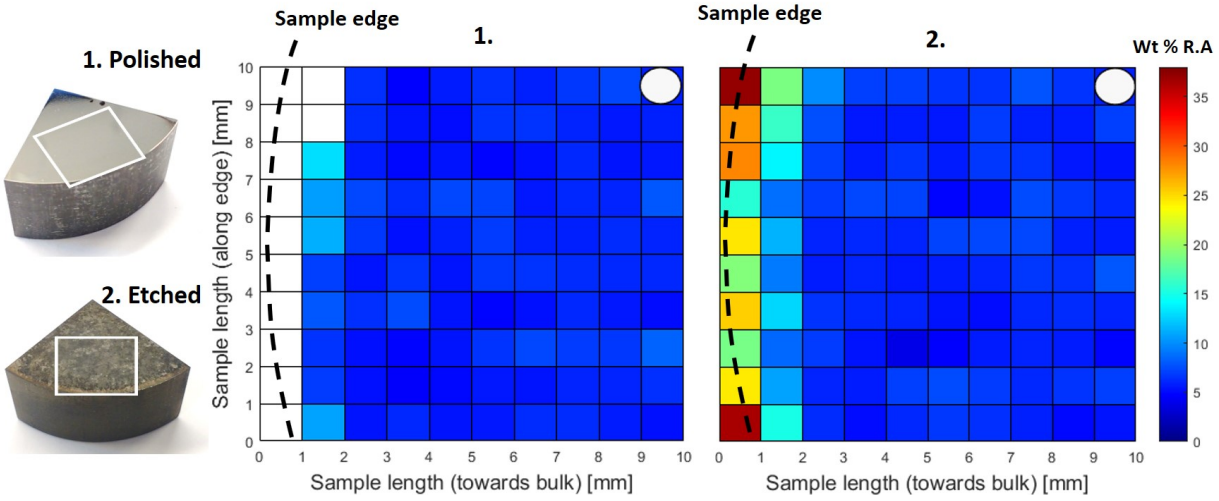

Figure 18: Two 10×10 SXRD phase maps of the polished (1) and etched (2) cross sections of a case-hardened steel bar showing the spatial distribution of retained austenite (R.A). The sample edge is indicated and the size of the XRD spot is shown in the top right corners.

Figure 19 displays three diffraction patterns from the sample after etching. The diffractograms are taken from 10, 2 and 1 mm away from the sample edge. For the two diffractograms closest to the edge, the austenite peaks have increased in intensity (most notably the A (200) peak), while the martensite peaks have decreased. It is this combined increase in austenite and decrease in martensite scattering which results in the drastic increase in the resulting wt% values for retained austenite (as seen in figure 18).

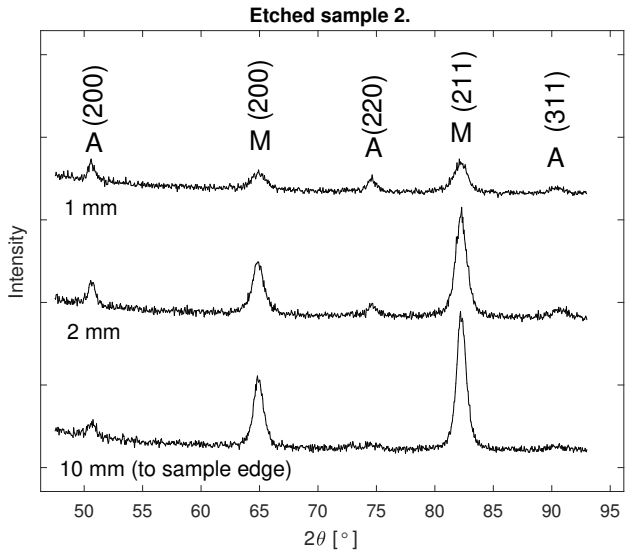

Figure 19: Three diffraction patterns from an approximate 1, 2 and 10 mm distance from the edge of the cross section of a polished steel bar after etching.

Figure 20 shows two steps in the refinement of the experimental data (dots) and theoretical model (line) from the SXRD map of the sample before etching. In 20a the unit cells, scale factors, zero shift and pseudo Voigt profile parameters were sequentially refined for both phases. By observing the fit however, the theoretical model does not fully incorporate the austenite (200) and martensite (211) peaks. This mismatch is an indication that the directional distribution of the microstructural grains in the sample is not random, i.e. that the sample microstructure has a preferred orientation or "texture". The deviation for the mentioned peaks indicate that the A (200) and M (211) atomic planes tends to be overrepresented in the planes that lie parallel to the sample surface, which are the planes from which scattering is recorded in a coupled 2θ measurement. Texture was included in the refinement process using the March-Dollase approach [18]. The resulting theoretical model is seen in figure 20b, where the austenite (200) and martensite (211) peaks better match the experimental data.

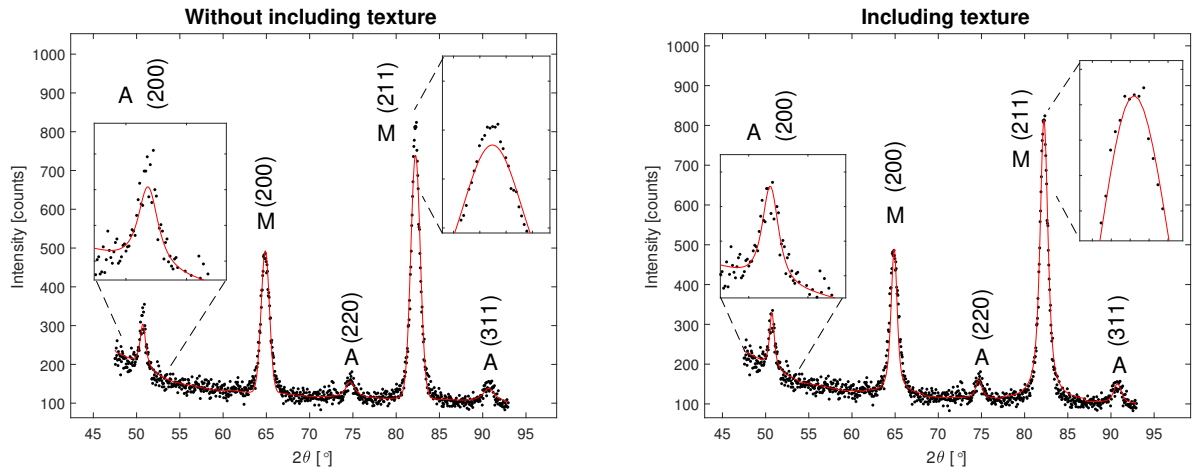

(a) (b)

Figure 20: The reference diffraction pattern with fitted theoretical data. The texture of the sample, visible for the M (211) peak and A (200) peak in (a) is refined. The result is plotted in (b) where the theoretical model better matches the experimental data.

To investigate the retained austenite gradient in the case-hardened region additional SXRD phase mapping was conducted with higher resolution (0.3 mm spot size). This resulted in 400 obtained diffractograms in a region of 3×12 mm. The phase distribution, from the same SXRD scan, is displayed in three color plots in figure 21, showing the individual phase scale factors for martensite (a) and austenite (b) together with the resulting wt% values for retained austenite (c). The martensite scale factors are consistent in their distribution across the rows of the SXRD map with decreasing values at 1 mm from the edge. In addition, they clearly reflect the roundness in the sample geometry. The austenite scale factors show, as expected, an increase in the carbon case hardened region, they are not however, evenly distributed. There seem to be smaller regions near the sample edge, with a higher concentration of retained austenite.

As discussed in the theory section, the scale factors for each phase represent the area of the corresponding Bragg peaks. They do not, in themselves, give a qualitative phase analysis and may vary due to differences in the scattering events across the sample. The relative scale factors however do represent individual phase fractions. Because of a strong decrease in the martensite scale factor for the last column to the left, the concentrated regions of retained austenite have shifted closer to the sample edge when comparing the phase fraction with the obtained wt% values. The retained austenite phase map is finally shown in figure 21d in the position of the SXRD scan on the sample. The color plot has been processed using image smoothing by interpolation.

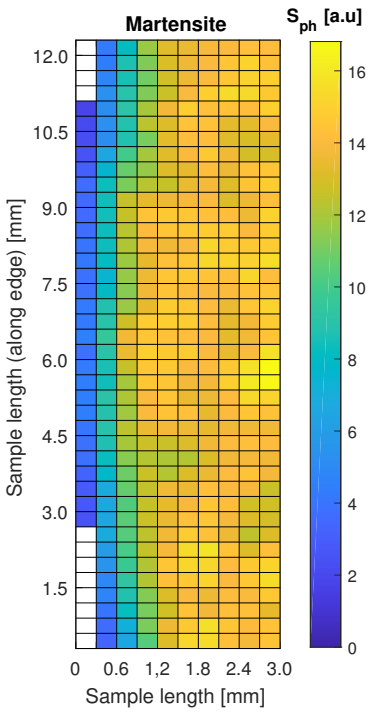

(a)

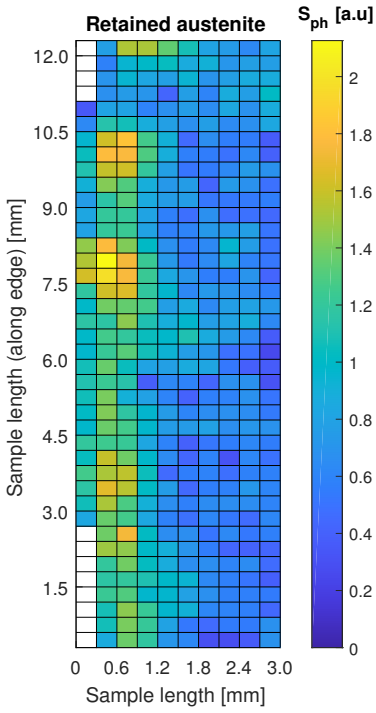

(b)

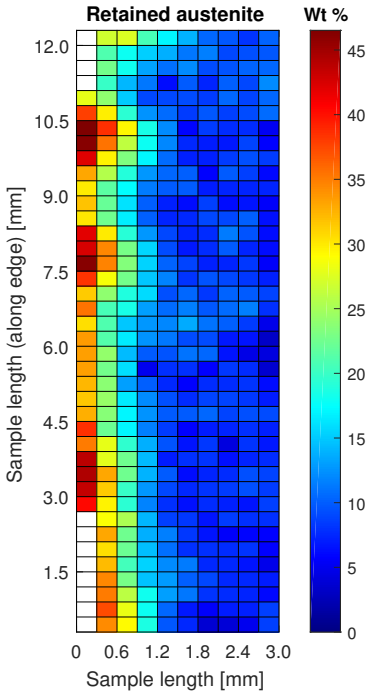

(c)

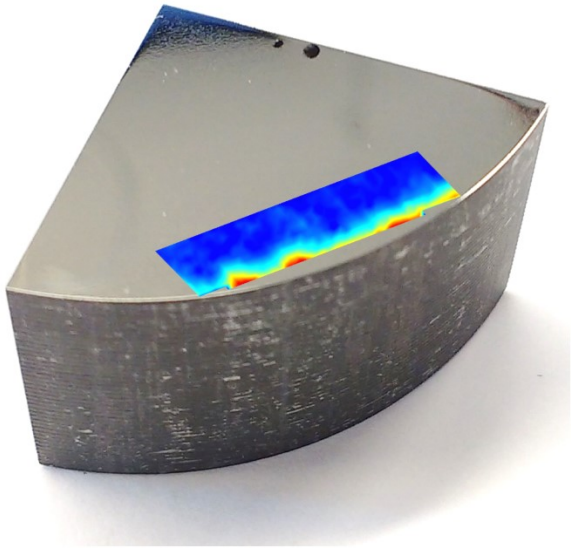

(d)

Figure 21: Three 40×10 phase maps of the same SXRD measurement of a 12×3 mm area of the cross section of a case-hardened steel bar. a) Martensite scale factors. b) Retained austenite scale factors. c) Retained austenite wt% vales. d) The smoothed retained austenite phase map in the position of the SXRD measurement.

The average scale factors obtained from the refinement process for each 10 columns in the 40×10 phase map matrix is displayed in figure 22a. The dramatic increase in wt% for retained austenite close to the sample edge, shown in the color plot (figure 18), is a result of the reducing scale factors for the martensite phase, from roughly 2 mm from the edge, combined with the increasing austenite factor in this region. The increase in austenite reaches a maximum at roughly 0.5 mm from the sample edge, as can be seen in the inset. The reduction of the martensite scale factors is not in itself an indication that the volume fraction of this phase is decreasing and could be attributed to a weaker signal around the sample edge. The fact that the austenite scale factors increase in the same region is an indication that the signal has not decreased, rather that the high carbon content close to the edge of the case-hardened steel bar has suppressed the martensite transformation during the carburizing process, leading to a high degree of retained austenite in this region [20].

The average wt% values for retained austenite is shown in figure 22b with a maximum value of 38%. In the inset an exponential function has been fitted to the wt% data which indicates that there is an exponential increase in the carbon concentration in the case-hardened region of the steel bar. The standard deviation for the wt% values increases with a decreasing distance to the edge. This is partly caused by the uneven concentration of retained austenite in this region and the difference in sample and map geometries causing the points on the same column to be located at varying distances from the sample edge.

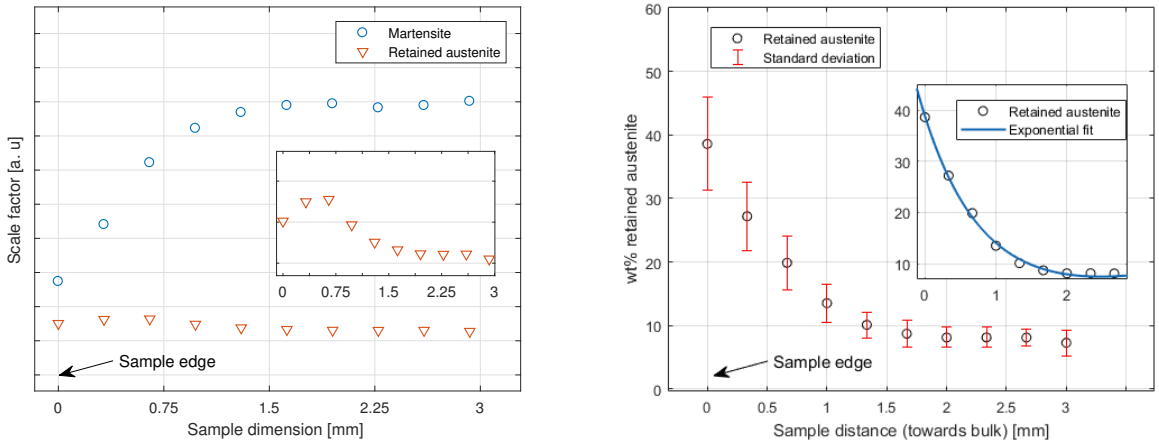

(a) (b)

Figure 22: a) The average scale factors for the martensite and retained austenite phases. The inset shows the increase in the austenite scale factors which peaks roughly 0.5 mm from the edge. b) The corresponding wt% values. The inset shows an exponential fit to the data.

4.2 Retained austenite in Q&P steel sheets

The mechanical stability of retained austenite in bend tested Q&P steel sheet samples was investigated using single "point" XRD measurements and SXRD phase mapping. Quantitative phase analysis was conducted to calculate the wt% values of retained austenite on four different pieces of the same steel which had been deformed to increasing strain values.

The results from the top and bottom of the bend (the tension and compression side) are plotted in figure 23 against increasing strain. Before bending there was 6.9 wt% retained austenite in the steel. For sample 1 (bend tested using the larger bending pin of 15 mm) the austenite content clearly decreases to 2.6 % on the compression side and 1.2 % on the tension side. For sample 2, the value drops slightly for the compression side and increases by 0.8% on the tension side. In comparison, the martensite transformation seems to be more extensive in the tension side of the bend.

For samples 3 and 4 a cut was induced from the loading pin, which is why measurements were only conducted on top of the bends. In addition, fracture occurred on top of sample 4. In both cases the austenite content dropped to zero indicating total martensite transformation.

In a similar study Kokosza and Pacyna showed the destabilization of retained austenite of low alloy structural steels under tensile testing [26]. They proposed that the mechanical stability of retained austenite increases with higher concentrations of carbon and other alloying elements in the steel, which hinders to the movement of dislocations in the crystal structure necessary to accommodate the martensite transformation. A low mechanical stability of retained austenite in Q&P sheet steels is however beneficial in many applications and industries since it increases the formability and energy absorption of the steel during deformation in transition induced plasticity (TRIP) effects [21].

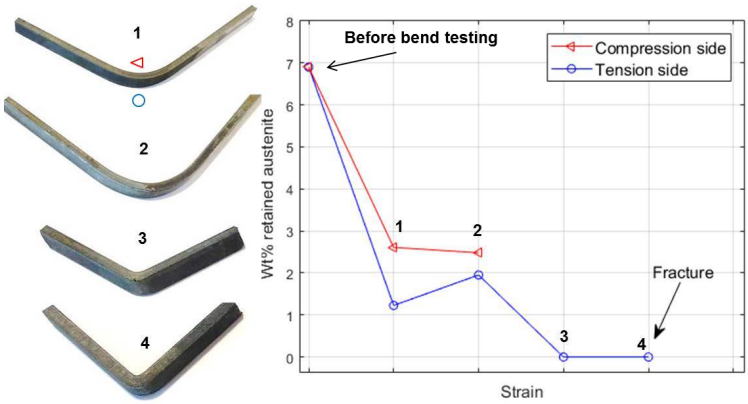

Figure 23: The evolution of the wt% retained austenite in bend tested Q&P sheet steels at increasing strains. Measurements were conducted on the tension and compressed side of the bends.

Figure 24 shows the diffractograms correlating to the calculated wt% values displayed in figure 23. In 24a the results from the four measurements on tension side are shown in addition to the diffraction pattern from a sample before bend testing. The initial diffractogram clearly contains the retained austenite (200) and martensite (200) peaks at 2θ values of 53 ° and 66° respectively, resulting in 6.9 % retained austenite by weight. For samples 1 and 2, which were bend with the larger 15 mm loading pin, there is a notable decrease in the austenite (200) peak. For samples 3 and 4, where fracture occurred on the tension side, the austenite peak is no longer distinguishable from the noise signal indicating a total martensite transformation. The reduction of the austenite peak seems to correlate with an increasing martensite peak. The increase in width is expected due to an increase of residual stresses in the material after bending, the increase in total peak area however is an indication of an increase in martensite volume fraction or a potential change in texture.

By comparing the diffractograms from the tension and compression side (figure 24b) the differences in the resulting wt% values shown in figure 23 can be identified. The A (200) peak is slightly larger and the M (200) peak smaller for the compression side for samples 1 and 2 indicating a higher austenite fraction. In addition, there has been a shift in peak positions in opposite directions for the two sides. This is caused by residual stresses in the material from the bend testing process, which causes contractions and extensions of the distance d between atomic planes in the sample microstructure. Since a coupled 2θ geometry was used no quantitative information about the residual stresses can be extracted from the diffraction patters which would require additional measurements using the $\sin^2\psi$ method [14].

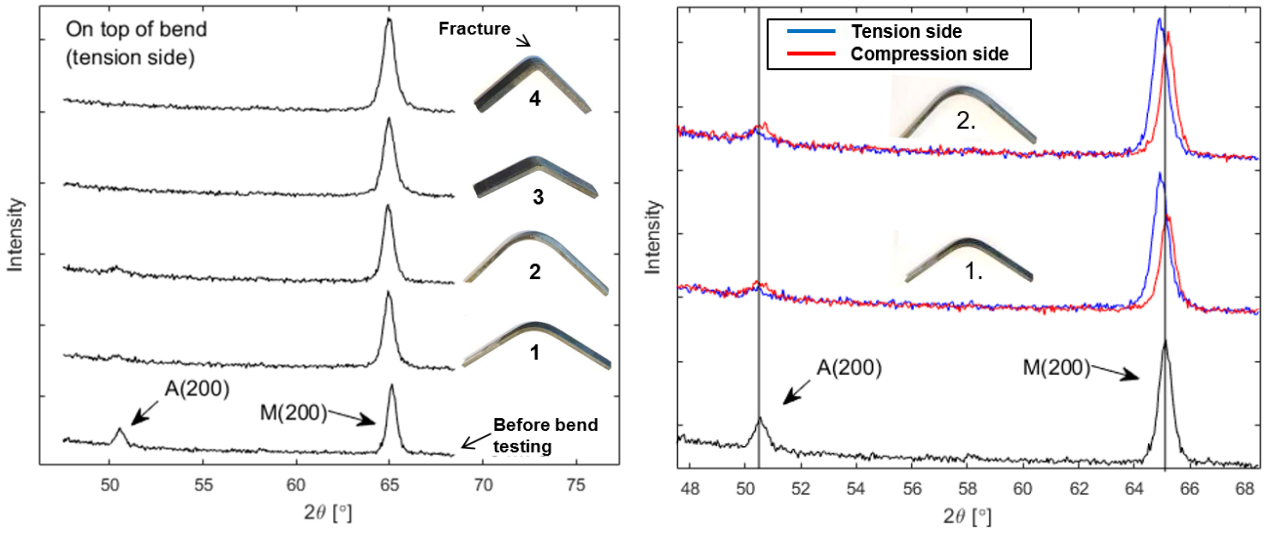

(a) (b)

Figure 24: XRD measurements on Q&P sheet steel samples after bend testing to increasing strains. a) On top of the bend (tension side). b) Comparison between the top and bottom of the bend (tension and compression side).

4.2.1 Cross section

The spatial distribution of retained austenite was further measured on the cross section of sample 2 using SXRD phase mapping. A 2.7×4.2 mm surface area was scanned using a XRD spot size of 0.3 mm. The obtained wt% values (between 1.7 and 8.1 %) are presented in a color plot in figure 25a. The majority of the XRD measurements on the first row, three on the 8th and all on the 9th were either too close to the edge of the sample or completely outside, such that the noise to peak ratios for the obtained diffraction patterns were too large to extract any valid information.

The color plot in figure 25a is further shown in the position of the scanned area of the bend in (b). Here it can be seen that the distribution of retained austenite is clearly not homogeneous across the width of the cross section. There seem to be an accumulation of retained austenite, between 5 % and 8 % in the compression side of the bend and less ($\sim$ 2 % to 5 %) in the tension side (the top part).

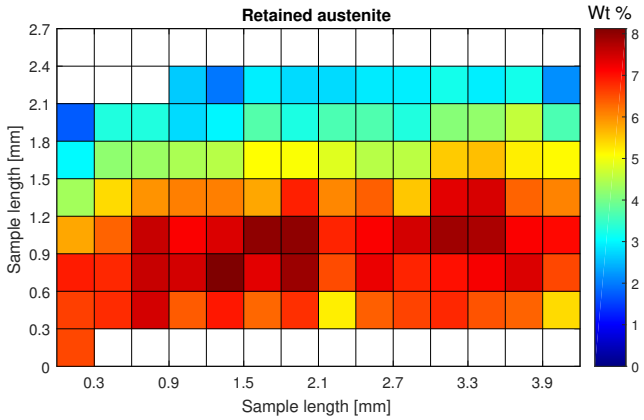

(a)

(b)

Figure 25: The spatial distribution of retained austenite over the cross section of a bend tested Q&P steel sheet sample. a) A color matrix representation of the obtained wt% values. b) The color matrix placed in the position of the scanned area on the cross section of the sample. The figure shows an uneven distribution of R.A with an accumulation in the compression side of the bend.

To illustrate the apparent gradient between low and high values of retained austenite through the cross section, the average values for each row of the scanned matrix is shown in figure 26. Here the bottom row is excluded since it only contains one out of 14 elements. The plot indicates that there is a clear increase in retained austenite from the tension side to the compression side. The maximum value (7.23±0.63 wt%) is however not located at the middle, rather closer to the compression side. This value corresponds to the forth row (starting from the bottom) of the color matrix displayed in figure 25a. The last value, obtained from the immediate vicinity of the compression side edge, shows a small decrease to 6.42±0.58 %. The large standard deviations may partly be due to small deviations in retained austenite along the cross section at equal distances to the sample edges. The main contributor however, is most likely the difference in sample and SXRD phase map geometry (as discussed in section 4.1.2).

In comparison with the single XRD measurements conducted on the top and bottom of

the bend of sample 2 (displayed in figure 23) there are some inconstancies in the obtained wt% values. The unbend region and the tension side (on top of the bend) contained 6.9 % and 2.3 % retained austenite which falls within the standard deviation of the maximum value obtained on the cross section of 7.2±0.6 % (where the least amount of austenite had transformed) and close to the tension side edge of 2.7±0.4 %. Close to the compression side however the values do not drop below 6.4±0.5 % as opposed to 2.5 % from the measurements under the bend. This inconsistency is likely due to a difference in sample preparation before the XRD measurements, in which the cross section was prepared with surface grinding using fine sandpapers (up to 3000-grit) while the top and bottom surfaces of the samples were prepared with rough grinding from an original sheet thickness of 4 mm.

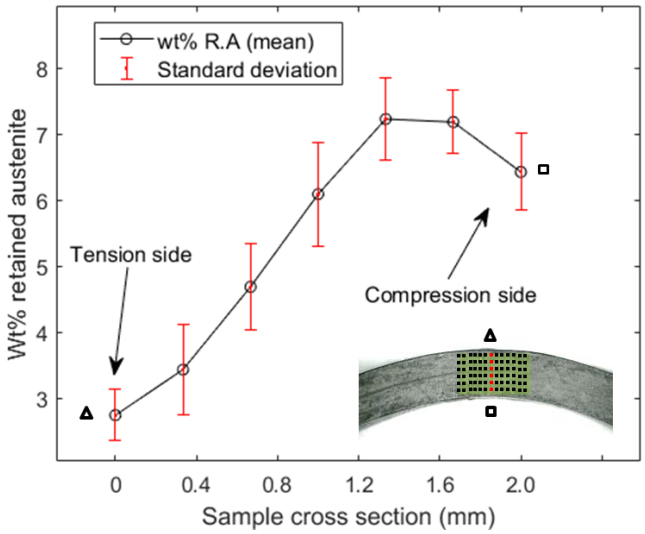

Figure 26: The mean wt% values of retained austenite from the tension to the compression side of the cross section of a bend tested Q&P steel sheet sample. The inset illustrates the location of the SXRD phase map.

The mechanical stability of retained austenite seems to differ for tensile and compressive loading conditions. The high mechanical stability of retained austenite in the compression side of the bend tested samples may be influenced by the inability of the microstructure to accommodate the volume expansion of the martensite transformation [27]. The strain followed by tensile stress however, would in contrary be more likely to accommodate this expansion.

5 Conclusion and outlook

In this thesis, a methodology for measuring microstructural variations in steel components using SXRD phase mapping has been established. This has been achieved using batch data processing and automated Rietveld refinements. The method has proven successful for a variety of martensitic steel samples with different geometries, including case hardened steel bars and bend tested Q&P steel sheets. In each case inhomogeneities in the distribution of retained austenite has been discovered and presented in simple 2D color plots.

Initially the cross section of two case hardened steel bars (labeled 1 and 2) were investigated, in which there are predicable differences in retained austenite distribution between bulk and carburized edges. A line scan over the cross section of steel bar 1 revealed a clear reduction of retained austenite from bulk values of 6-14 % to 0% starting at a distance of $\sim$ 8 mm from the edges. The results indicated a depletion of carbon around the steel bar from a possible decarburizing process during manufacturing. In addition, SXRD phase mapping was conducted over the cross section of steel bar 2. Two 10×10 mm phase maps revealed small deviations of $\sim$ 1% in bulk values of retained austenite with 6.0±0.8 wt% prior to and 6.3±0.9 wt% after etching. An increase in austenite was seen in the case hardened region around the sample edge, which was further investigated using a higher SXRD resolution. The results indicated an exponential increase in retained austenite content from a distance of $\sim$ 2 mm from the sample edge. In addition retained austenite was found to be concentrated in regions of roughly 1×1 mm in proximity to the edge.

The method was also used to study the mechanical stability of retained austenite in 4 Q&P steel sheet samples which were bend tested prior to measurements. Initially single XRD measurements were conducted on the top and bottom of the bends (tension and compression side). A trend of decreasing austenite content could be found from 6.9 wt% before bending to 0 wt% after fracture (on top of the bend). Additionally, the distribution of retained austenite over the cross section of sample 2 was investigated. Here it could be seen that the stability of the austenite is lower at the tension side of the bend which contained between 2 and 5 wt%. The compression side contained higher values (between 5 and 8 wt%) which indicates that the stress induced by compression may inhibit the volume expansion of the martensite transformation.

To further develop the methodology presented in this thesis there are a few recommendations for future work. To improve the quality of the generated least squares fits, the profile and texture parameters could be included in the automated refinement process using additional refinement cycles, as described by Birkedal and Frølich [5]. This could potentially account for variations in texture, strain and other microstructure deviations across the sample which

effect the profile of the obtained Bragg peaks. Additionally, the rounded sample geometry in the samples proved challenging when generating square SXRD phase maps. Close to the edges the XRD spot completely or partly missed the sample. In this way it it hard to estimate the position of the measured point in relation to the edge. By introducing possible variations in the geometry of the SXRD grids this problem could be solved. This may however complicate the subsequent computer analysis process.

Regarding the measurements conducted on the Q&P sheet steels, there are additional steps required to verify and further investigate the discovered inhomogeneity in the distribution of retained austenite. By generating additional SXRD phase maps of samples before bending and bended to higher strains (such as samples 3 and 4), the evolution of the martensite transformation could be investigated. Furthermore, by measuring the cross section of thicker samples, more XRD points could be included in the phase maps, thus increasing the accuracy of the measurement.

In conclusion, the methodology presented in this thesis can further be used to characterize macroscopic phase distributions in other metals or solids. This has been shown to be possible using a lab diffractometer and subsequent automated Rietveld refinements.

References

[1] Authier A: *Early Days of X-ray Crystallography*, Oxford scholarship online (2013)

[2] Rietveld H.M. *A profile refinement method for nuclear and magnetic structures*, J. Appl. Cryst. 2, 65-71 (1969)

[3] Elmer W.J et al. *Spatially resolved X-ray diffraction phase mapping and $\alpha \rightarrow \beta \rightarrow \alpha$ transformation kinetics in the heat-affected zone of commercially pure titanium arc welds*, Metallurgical and materials transactions A, Vol. 29 A; 2761 (1998)

[4] Chahine G.A et al: *Imaging of strain and lattice orientation by quick scanning X-ray microscopy combined with threedimensional reciprocal space mapping*, J. Appl. Cryst. 47, 762–769, (2014)

[5] Frølich S. and Birkedal H: *MultiRef: software platform for Rietveld refinement of multiple powder diffractograms from in situ, scanning or diffraction tomography experiments*,J. Appl. Cryst. 48, 2019–2025 (2015)

[6] Waseda Y. et al: *X-Ray Diffraction Crystallography Introduction, Examples and Solved Problems*, Springer (2011)

[7] Jatczak C.F: *Retained Austenite and Its Measurement by X-Ray Diffraction*,Society of automotive engineers SAE, 800426 (1980)

[8] Mittemeijer E. J: *Fundamentals of Materials Science: The Microstructure–Property Relationship Using Metals as Model Systems*, Springer (2010)

[9] Dossett J.L. and Boyer H.E: *Practical Heat Treating, Second Edition*, ASM International (2006)

[10] Brog J-P. et al: *Polymorphism, what it is and how to identify it: A systematic review*, RSC Advances, DOI: 10.1039/c3ra41559g (2013)

[11] Als-Nielsen J. and McMorrow D. *Elements of Modern X-ray Physics*, John Wiley & Sons, second edition (2011)

[12] Poly Crystallography, inc. [Internet]: [Cited *August*12, 2018] Available from: http://www.polycrystallography.com/XRDanalysis.html

[13] Larson A.C. and Von Dreele R.B: *General Structure Analysis System (GSAS)* Los Alamos National Laboratory Report LAUR 86-748 (2004).

[14] Fitzpatrick M.E. et al: *Determination of Residual Stresses by X-ray Diffraction – Issue 2*, National Physical Laboratory, Measurement Good Practice Guide No. 52 (2005)

[15] Kaduk J.A and Reid J: *Typical values of Rietveld instrument profile coefficients*, Powder Diffraction 26, 1, (2011)

[16] Toraya H. *A new method for quantitative phase analysis using X-ray powder diffraction: direct derivation of weight fractions from observed integrated intensities and chemical compositions of individual phases*, J. Appl. Cryst. 49, 1508-1516 (2016)

[17] Crystallography Open Database [Internet]: [cited August 12, 2018]. Available from: http://www.crystallography.net/cod/

[18] Dollase W. A. *Correction of intensities for preferred orientation in powder diffractometry: application of the March model*, J. Appl. Cryst. 19, 267-272 (1986).

[19] The MathWorks Inc: *MATLAB version 2017a*, Natick, Massachusetts, (2017)

[20] Parrish G: *Carburizing: Microstructures and Properties*, ASTM International 10.1361 (1999)

[21] Speer J.G. et al: *The "Quenching and Partitioning" Process: Background and Recent Progress*, Materials Research, Vol. 8, No. 4, 417-423 (2005)

[22] Hossain R. et al: *Stability of retained austenite in high carbon steel under compressive stress: an investigation from macro to nano scale*, Scientific Reports, 6, 34958 (2016).

[23] Mak P: *Piranha Clean Procedure*, Boston University Photonics Center, (2010)

[24] Bruker [Internet]: [Cited $August 12, 2018$] Available from: https://www.bruker.com/products/x-ray-diffraction-and-elemental-analysis/x-ray-diffraction/d8-discover-family.html

[25] Ball C. J. and Kelly P.M: *X-ray method for determination of retained austenite in steels with pronounced texture*, Metal science, Vol. 16, 332-334 (1982)

[26] Kokosza A. and Pacyna J: *Mechanical stability of retained austenite in unalloyed structural steels*, Archives of metallurgy and materials, Vol. 55, No. 4, 1001–1006 (2010)

[27] Hidalgo J. et al: *Thermal and mechanical stability of retained austenite surrounded by martensite with different degrees of tempering*, Materials Science & Engineering A, 690, 337–347 (2017)